Electric Power Systems Research 209 (2022) 107968

Contents lists available at ScienceDirect

Electric Power Systems Research

journal homepage: www.elsevier.com/locate/epsr

# Precise ROCOF estimation algorithm for low inertia power grids

He Yin [a,*], Yuru Wu [a], Wei Qiu [a,*], Chujie Zeng [a], Shutang You [a], Jin Tan [c], Andy Hoke [c], Cameron J. Kruse [d], Brad W. Rockwell [d], Kelcie Ann Kawamura [e], Yilu Liu [a,b]

[a] Department of Electrical Engineering and Computer Science, The University of Tennessee, Knoxville, TN, 37996, USA
[b] Oak Ridge National Laboratory, Oak Ridge, TN, 37831, USA
[c] National Renewable Energy Laboratory, Golden, CO, 80401, USA
[d] Kauai Island Utility Cooperative, Lihue, HI, 96766, USA
[e] Hawaiian Electric Company, Inc, Honolulu County, HI, 96813, USA

ARTICLE INFO

*Keywords:*
Rate of change of frequencies
Synchronized measurement devices
Event capturing
Low inertia power system
Frequency estimation

ABSTRACT

The precise estimation of Rate Of Change Of Frequencies (ROCOFs) in a generation trip event can be helpful on power system inertia estimation, fast system response, and accurate event capturing. However, the ROCOF estimations from the existing Synchronized Measurement Devices (SMDs) are usually simply calculated by the finite difference between two adjacent frequency measurement points. The ineluctable noises, disturbances, and spikes from real-world frequency measurements can bring large dynamics to the ROCOF estimation and thus can result in an inaccurate estimation of the initial ROCOF. This issue becomes more serious when the target power grid has low inertia and a large amount of distributed energy sources are deployed. To address this issue, a precise ROCOF estimation algorithm is designed based on least square method with flexible window size. In addition, a median filter is also designed and applied on the frequency measurements before using the proposed algorithm. The window size and thresholds in the proposed algorithm are determined with historical event data analysis. The proposed algorithm is deployed in a low cost, flexible, and distribution level universal grid analyzer (UGA) platform. Multiple experiments are conducted in both a laboratory and the Hawaiian Islands to verify the effectiveness of the proposed algorithm.

## 1. Introduction

Rate Of Change Of Frequencies (ROCOFs) measured from Synchronized Measurement Devices (SMDs) have critical contributions to the power system applications such as inertia estimation [1,2], frequency control [3], protection [4], and event detection [5]. For example, the ROCOF could be an essential measurement for fast frequency control in a low inertia power system. ROCOFs are also critical measurements for oscillation detection [6]. It would be more important when the power system contains large amounts of distributed energy sources (DERs). However, the dynamics generated from DERs may bring disturbances on the frequency measurements and thus results in inaccurate ROCOF measurements.

According to IEEE C37.118.1 [7], SMDs are required to provide ROCOF measurements. However, there is no specific ROCOF measurement algorithm requirement in this standard. The simplest ROCOF calculation approach is to calculate the finite difference between two adjacent frequency measurements [8]. In contrast, in real-world applications, the ineluctable noises, disturbances, and spikes from the frequency measurements can bring challenges to the precise ROCOF estimation. Wright et al. [9] introduces one of the significant problems with ROCOF estimation which is the phase steps or phase jump. The phase steps cause frequency spikes and thus cause ROCOF spikes. In order to remove the fast ROCOF dynamics, [10] introduces an interpolated Discrete Fourier Transform (DFT) and Kalman filter method to precisely estimate ROCOF. Unfortunately, this method cannot be applied in real-time. Frigo et al. [11] utilizes a low-pass filter to the ROCOF measurements to provide a smoother trend. In addition, the ROCOF estimation algorithms can be either non-window based or window based ones. For non-window based algorithms, the enhanced interpolated DFT [12] and the iterative interpolated DFT [13] are two static estimation algorithms which only compute the ROCOF as the incremental ratio between two adjacent frequency points. On the other hand, window based algorithms provide a more accurate ROCOF estimation such as compressive sensing-based TaylorFourier model [14]. However, the window sizes of window based algorithms can be different

* Corresponding authors.
*E-mail addresses:* hyin8@utk.edu (H. Yin), qwei4@utk.edu (W. Qiu).

https://doi.org/10.1016/j.epsr.2022.107968
Received 3 December 2021; Received in revised form 4 March 2022; Accepted 24 March 2022
Available online 30 March 2022

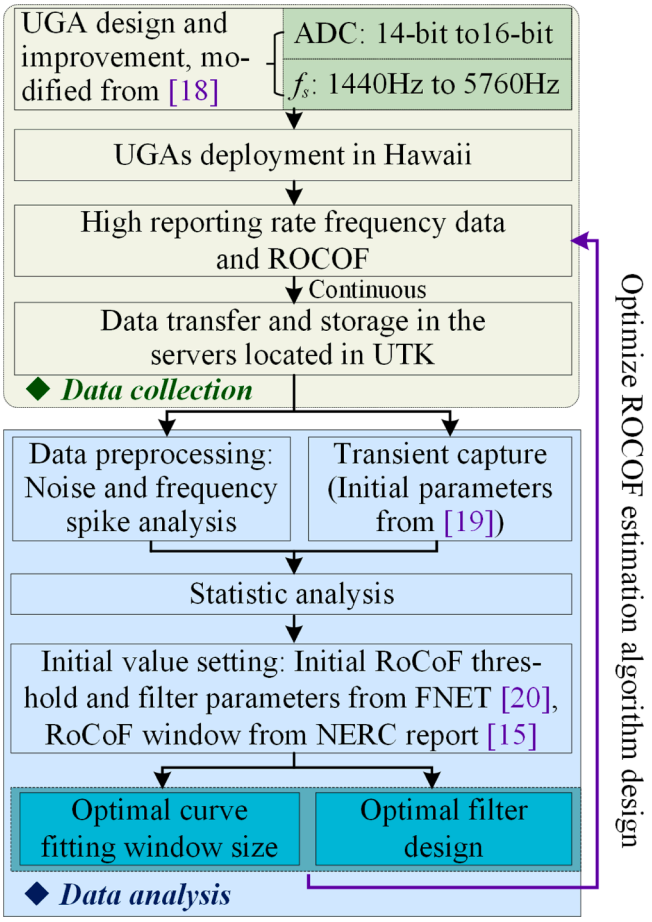


**Fig. 1.** Framework of the Precise ROCOF estimation algorithm.

based on ROCOF applications and the system inertia of the target power grid.

The recommended ROCOF estimations in the power grids with large inertia are with 0.1 to 0.5 s window sizes [15]. The ROCOF estimation problem becomes especially difficult when the scale of the power grids become smaller or when the level of non-synchronous generation becomes very high since the system inertia become smaller. For example, [16] uses multiple window sizes, i.e., 0.1, 0.25 and 0.5 s, for ROCOF estimation in a power grid with a battery energy storage system deployed while [17] uses a 0.1 s window size for ROCOF estimation since their target power grid is a microgrid with low inertia. Moreover, with more renewable energy sources deployed, the system inertia would become even smaller and thus further increase the difficulty of the ROCOF measurement accuracy. On the other hand, if the ROCOF window size becomes too small, the breaker operations and noises may also trigger the event detection.

To address the precise ROCOF estimation in low inertia power grids, this paper aims to precisely measure the ROCOF in real-time with low inertia power grids. In order to measure ROCOFs, a precise DFT based frequency measurement algorithm with a high reporting rate is firstly introduced. Then, the least square method based ROCOF estimation algorithm with flexible window size is given. The window size and thresholds in the proposed algorithm are determined with historical event data analysis recorded from two Hawaiian Islands. To verify the real-world performance, the proposed algorithm is deployed in a low cost, flexible, and distribution level universal grid analyzer (UGA) platform. Finally, to verify the effectiveness of the proposed algorithm, multiple experiments are conducted in both a laboratory and the Hawaiian Islands.

The main contributions of this paper are summarized:

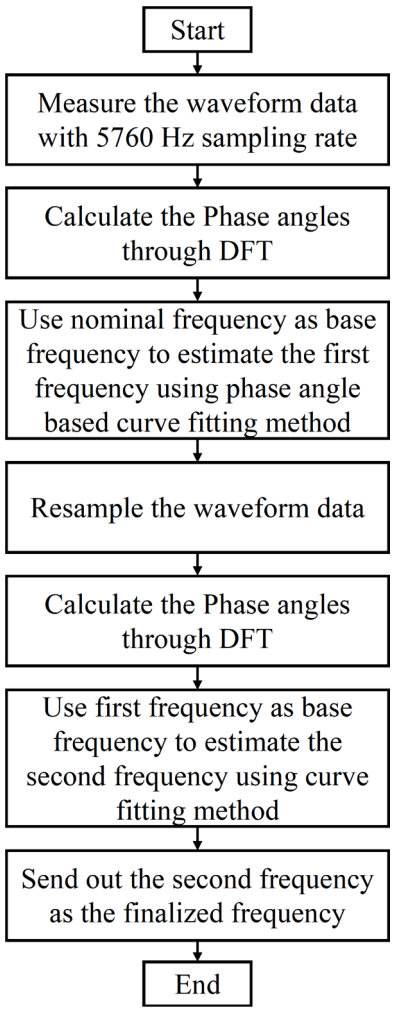


**Fig. 2.** Flowchart for the frequency estimation.

- A precise Rate Of Change Of Frequency (ROCOF) estimation algorithm is proposed through utilizing least square method with flexible window size and median filter.
- An event detector is designed and utilized to analyze the real-world transients captured from the Hawaiian Islands. Three kinds of events are successfully captured and categorized. The parameters in the ROCOF estimation algorithm are optimized through using event based statistic analysis.
- The real-world performance of the proposed algorithm is verified through deployment in a low cost, flexible, and distribution level universal grid analyzer platform. The accuracy of both frequency and ROCOF estimations are verified under steady state and wall sources.
- Multiple experiments are conducted both in the laboratory and in the Hawaiian Islands to verify the effectiveness of the proposed algorithm.

## 2. Precise ROCOF estimation algorithm

The overall framework of the proposed precise ROCOF estimation algorithm design is illustrated in Fig. 1. The first part is the data collection including UGA design and improvement, UGA deployment with high reporting frequency and ROCOF, and data transferring and storage. Then, in the second part, the data will be utilized to optimize the proposed algorithm design through an offline analysis including data preprocessing, transient capture, statistic analysis, initial value setting, optimization for curve fitting window size, and filter design. The relationship between the proposed work and previous work is marked out

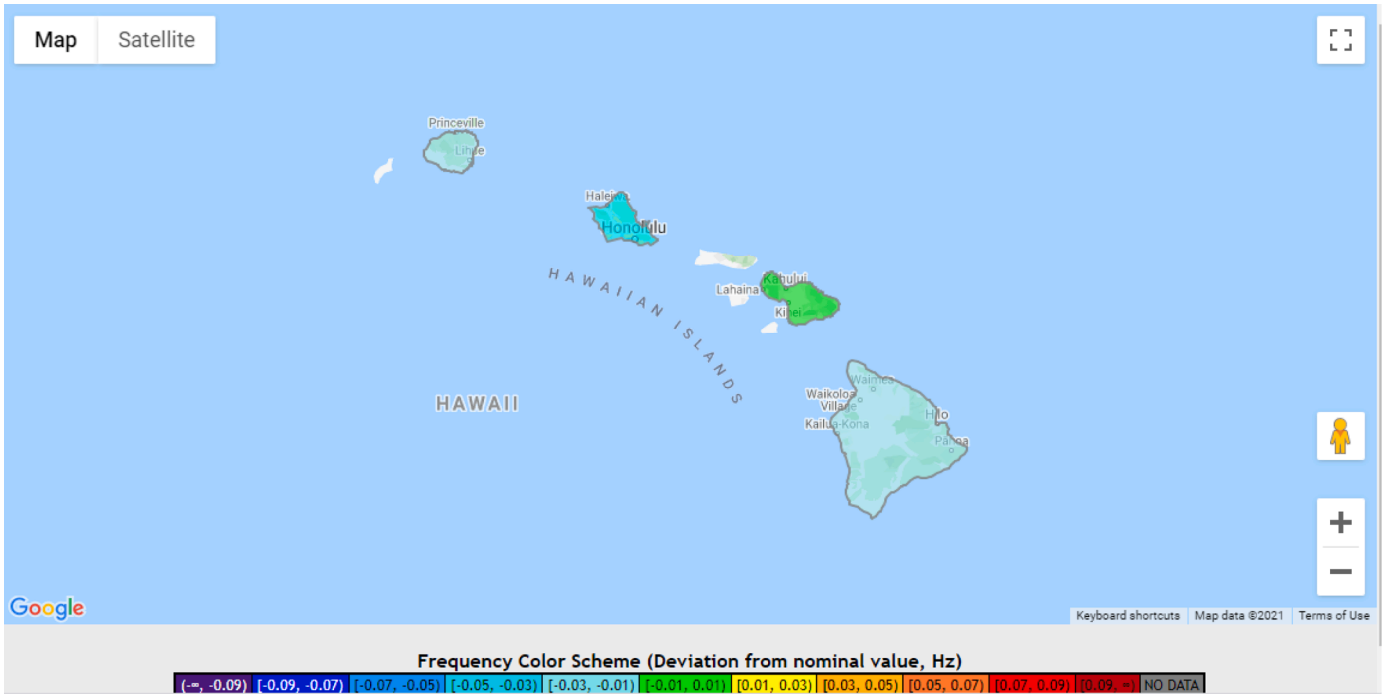


**Fig. 3.** FNET public website for Hawaiian Islands.

and detailed introduction for these steps will be given in the following sections.

### 2.1. Frequency estimation algorithm

A precise frequency estimation algorithm is the foundation of the precise ROCOF estimation. In this paper, a dynamic single-phase synchronized frequency estimation is used [18]. Since the detailed frequency estimation algorithm can be found in [18], only the flowchart for the frequency estimation is given in Fig. 2. Since the proposed ROCOF estimation algorithm is designed to be deployed in low inertia power systems, the system inertia will be much smaller than that of a large power grid. In this case, the frequency arresting period (before frequency drops to the Nadir) would be much shorter which requires a high frequency reporting rate for fast frequency control purposes. In this paper, As shown in Fig. 1, it can be seen that an improved UGA is designed during the data collection step, where the ADC is increased from 14-bit to 16-bit and the sampling rate is increased from 1440Hz to 5760 Hz. Besides, in the data analysis step, the initial parameters are set based on the literature listed in Fig. 1. Referring to the previous research, the initial parameters of transient capture, ROCOF threshold, filter, and ROCOF window are set from Zhan et al. [19], FNET [20], and Arana et al. [15], respectively. Then the optimal parameters of the proposed method are set through the experiments. In addition, a 120 Hz reporting rate is used for both frequency and ROCOF estimations. The reason for using 5760 Hz sampling rate is to have 96 samples per cycle so that the estimation accuracy of the phase angle can be increased. The frequency is estimated through using 24 phase angles with a second order curve fitting method [18]. In this case, precise phase angle measurements can increase the accuracy of estimated frequencies.

### 2.2. ROCOF estimation algorithm

A ROCOF is typically defined as the tangential line for any given point on a frequency response curve. From the SMDs' point of view (according to the IEEE C37.118.1 [7]), the definition of ROCOF is,

$$ROCOF(t) = \frac{df(t)}{dt}, \tag{1}$$

where $t$ is the time stamp and $f(t)$ is the frequency at time $t$. However, the $dt$ here can be a different value determined by the ROCOF estimation window size and frequency reporting rate. The ROCOF estimation algorithm is also not clearly defined. Usually, ROCOF estimated in the PMUs is using the smallest $dt$, i.e., calculate the ROCOF based on two adjacent frequency measurements and the frequency reporting rate.

### 2.3. Initial ROCOF estimation algorithm

The initial ROCOF is most commonly calculated as the change in frequency over 0.1 to 0.5 s right after a sudden generation trip or load change. Therefore, the initial ROCOF can be calculated as,

$$ROCOF_{initial}(t) = \frac{f_t - f_{t-\Delta t}}{\Delta t}, \tag{2}$$

where $\Delta t$ can range from 0.1 to 0.5 s [15]. However, directly using two frequency measurements to calculate the initial ROCOFs will result in a low precision on the ROCOF estimation. In this paper, a first order curve fitting method is applied to the frequencies over $\Delta t$ to estimate the ROCOF at $t + \frac{\Delta t}{2}$. Considering this method will be utilized in the real-world SMDs, the Least Squares Method (LSM) is utilized [21]. Assuming the time stamps of the frequency measurements to be $X$, the frequency curve $Y$ can be written as,

$$Y = k \cdot X + b, \tag{3}$$

where $k$ is the slope and $b$ is the intercept. Here, $k$ is the best fitted ROCOF with frequency curve $Y$. $k$ can be calculated as,

$$k = \frac{\overline{XY} - \overline{X} \cdot \overline{Y}}{\overline{X^2} - (\overline{X})^2}. \tag{4}$$

Since $\overline{X}$, $\overline{X^2}$, and $(\overline{X})^2$ are constant values and can be calculated before the real-time ROCOF calculation. For example, $X$ can be $[0, 1/120.2/120, \ldots, 12/120]$ if $\Delta t$ is 0.1s and the frequency reporting rate is 120 Hz.

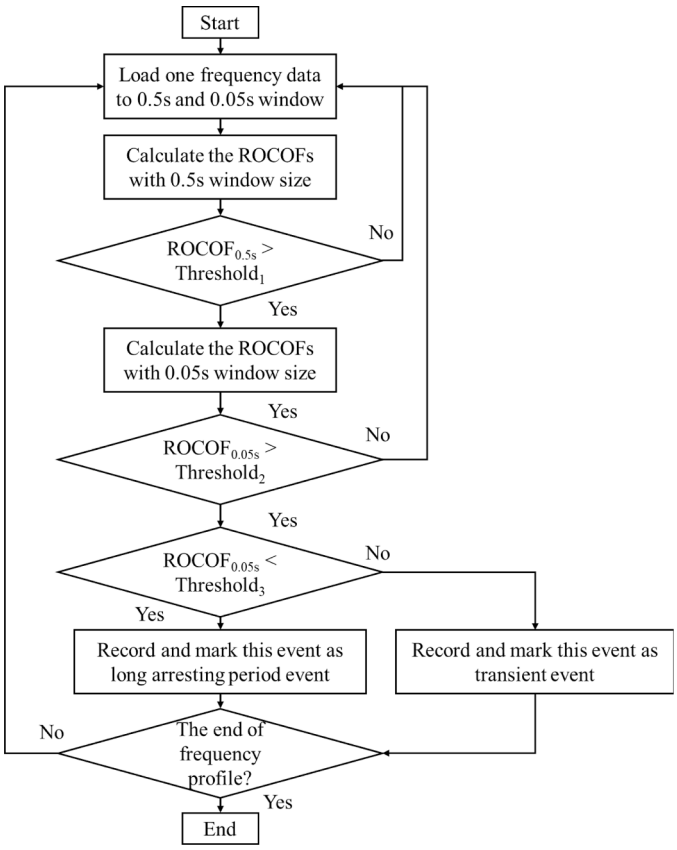


**Fig. 4.** Flowchart for event detection algorithm.

Note that $X$ should be determined based on the $\Delta t$ which is usually designed between 0.1 to 0.5 s.

## 3. Event detection algorithm

To further optimize the parameters in the proposed ROCOF estimation algorithm, two Universal Grid Analyzers (UGAs) have been deployed in the Hawaiian Islands, i.e., Maui and Kauai. Currently, they are streaming data back to the FNET Grideye [22] with a 120 Hz frequency reporting rate which is the highest frequency reporting rate mentioned in [23]. These two units are also available on the FNET public website in [20]. An illustration for the public data on the FNET public website is also given in Fig. 3. The different colors show the frequency deviation from the nominal value.

In order to design the $\Delta t$ in (2), the load change and generation trip events should be filtered out from the Hawaiian Island data. The event detection algorithm utilized in this work is a two filter based event detection algorithm. The flowchart of the proposed algorithm can be found in Fig. 4. Two ROCOF filters are designed with 0.5 and 0.05 s window sizes which are initially designed based on experience. Note that the window sizes are user defined values and will be revised based on the event analysis. Using different window sizes would have different ROCOF values and thus result in different threshold values. The three threshold values for UGA #2005 (located in Maui) and UGA #2006 (located in Kauai) are listed in Table 1. The threshold values for two units are different because the power system inertia for Maui is larger than that for Kauai.

## 4. ROCOF and filter window size design

### 4.1. Real-world event capturing and analysis

In order to finalize the $\Delta t$ in (2), the recorded events have been categorized into three groups based on the event arresting period: 1) transient events; 2) long arresting period events; and 3) hybrid arresting period events. The definition of the event arresting period is the time frame leading up to the nadir. As shown in Fig. 5, the event arresting period distribution is given sorting from the lowest value to the highest value. There are about 13 events with short arresting periods (transient events) and the rest are with long arresting periods. Examples of both transient and long arresting period events are given in Fig. 6(a) and (b). However, there are some events that have both transient and long arresting periods but are categorized into a transient event group. These events are now defined as hybrid period events, shown in Fig. 6(c). The causes of events are also confirmed with the local utility company: 1) transient events are usually breaker operation; 2) long arresting period events are usually load change or generation trip; 3) hybrid arresting period events are usually generation trip with fault. Note that this is a unique feature for a power system with low inertia. The generation trip events in large power system usually do not have the frequency spikes [5].

A summary for the event capturing results in two months is given in Table 2. The event capturing starts on June 11, 2021 and the data analyzed in this study ends on August 8, 2021. Based on the algorithm shown in Fig. 4, the transient and long arresting period events can be classified. Note that the initial parameters of the event capturing algorithm is coming from FNET event detection algorithm [6]. However, the hybrid arresting period events are hidden in the transient events which need eyeballing to pick them out. In addition, the hybrid arresting

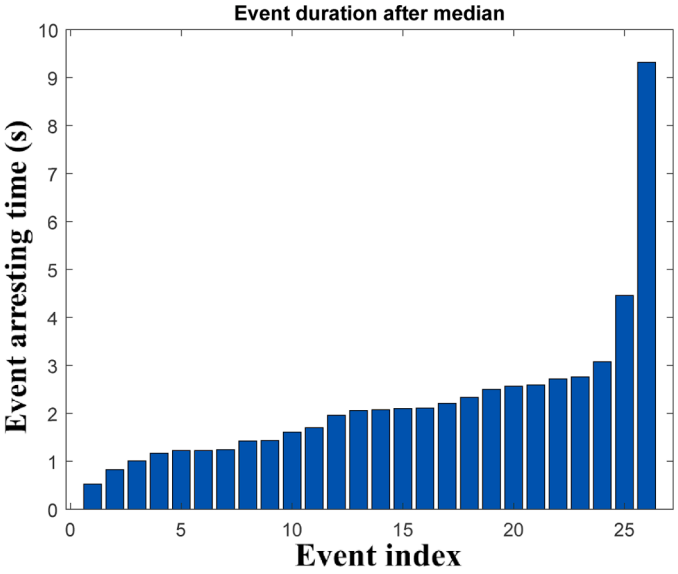


**Fig. 5.** Event arresting periods for one island.

**Table 1**
Threshold values for event detection.

| UGA # | Initial Threshold 1 | Initial Threshold 2 | Initial Threshold 3 | Final Threshold 1 | Final Threshold 2 | Final Threshold 3 |
|---|---|---|---|---|---|---|
| #2005 | 0.1 Hz/s | 0.25 Hz/s | 3 Hz/s | 0.1082 Hz/s | 0.1864 Hz/s | 1 Hz/s |
| #2006 | 0.2 Hz/s | 0.5 Hz/s | 6 Hz/s | 0.1895 Hz/s | 0.3822 Hz/s | 2 Hz/s |

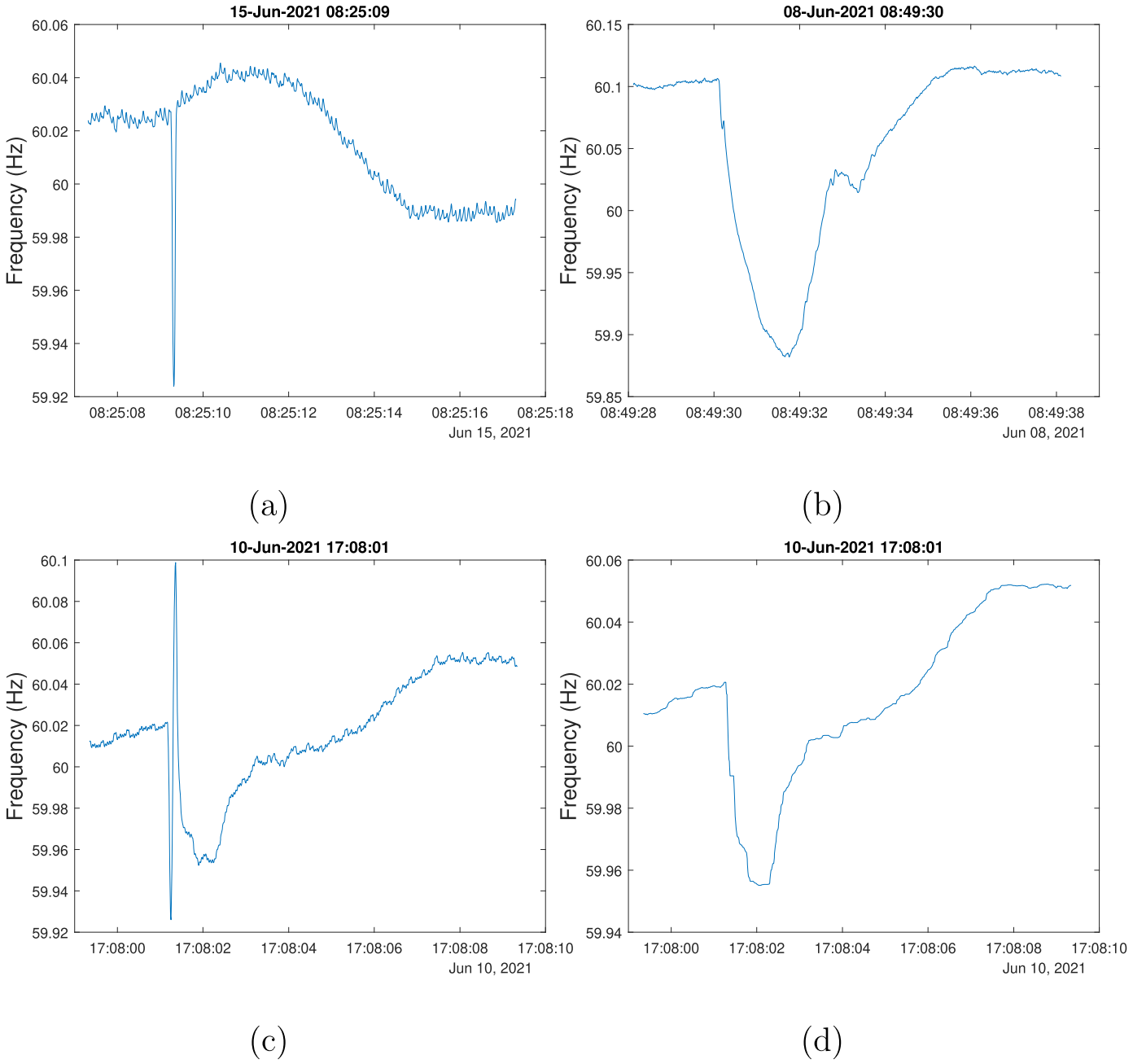


**Fig. 6.** Example events: (a) A transient event; (b) A long arresting period event; (c) A hybrid arresting period event; (d) A hybrid arresting period event after filtering.

**Table 2**
Event summary for two UGAs.

| UGA # | Deployed location | Transient events | Long arresting period events | Hybrid arresting period events |
|---|---|---|---|---|
| #2005 | Maui Island | 23 | 16 | 10 |
| #2006 | Kauai Island | 10 | 34 | 11 |

period events may have an inaccurate ROCOF with both 0.5 and 0.05 s ROCOF window sizes. Since the target events of this paper are the long arresting period events and the hybrid arresting period events, a median filter is utilized on the frequency response to filter out the frequency spikes. Based on the existing hybrid and long arresting period events, the median filter window size is designed to be $\frac{1}{3}$ s. The example hybrid arresting period event after filtering is given in Fig. 6(d).

In order to finalize the window size for the ROCOF estimation, the event arresting period for long arresting period events are calculated as,

$$T_{event} = T_{end} - T_{start}, \tag{5}$$

where $T_{end}$ and $T_{start}$ are the time stamps when frequency drop to 95% and 5% of the frequency nadir. The event arresting period for one island is shown in Fig. 5. It can be clearly observed that the minimum event arresting period which can be utilized is for the ROCOF window size design. By analyzing the ROCOFs of the transient events, the minimum event arresting period is also utilized for the second ROCOF window size design. Based on the above analysis, the two ROCOF windows are designed as 0.3 and 0.05 s. However, using the frequency responses after median filter will cause another issue that the ROCOF values become smaller. This means the ROCOF thresholds need to be adjusted to capture all the long and hybrid arresting events. Then the ROCOF thresholds are redesigned by analyzing the minimum and maximum ROCOFs with

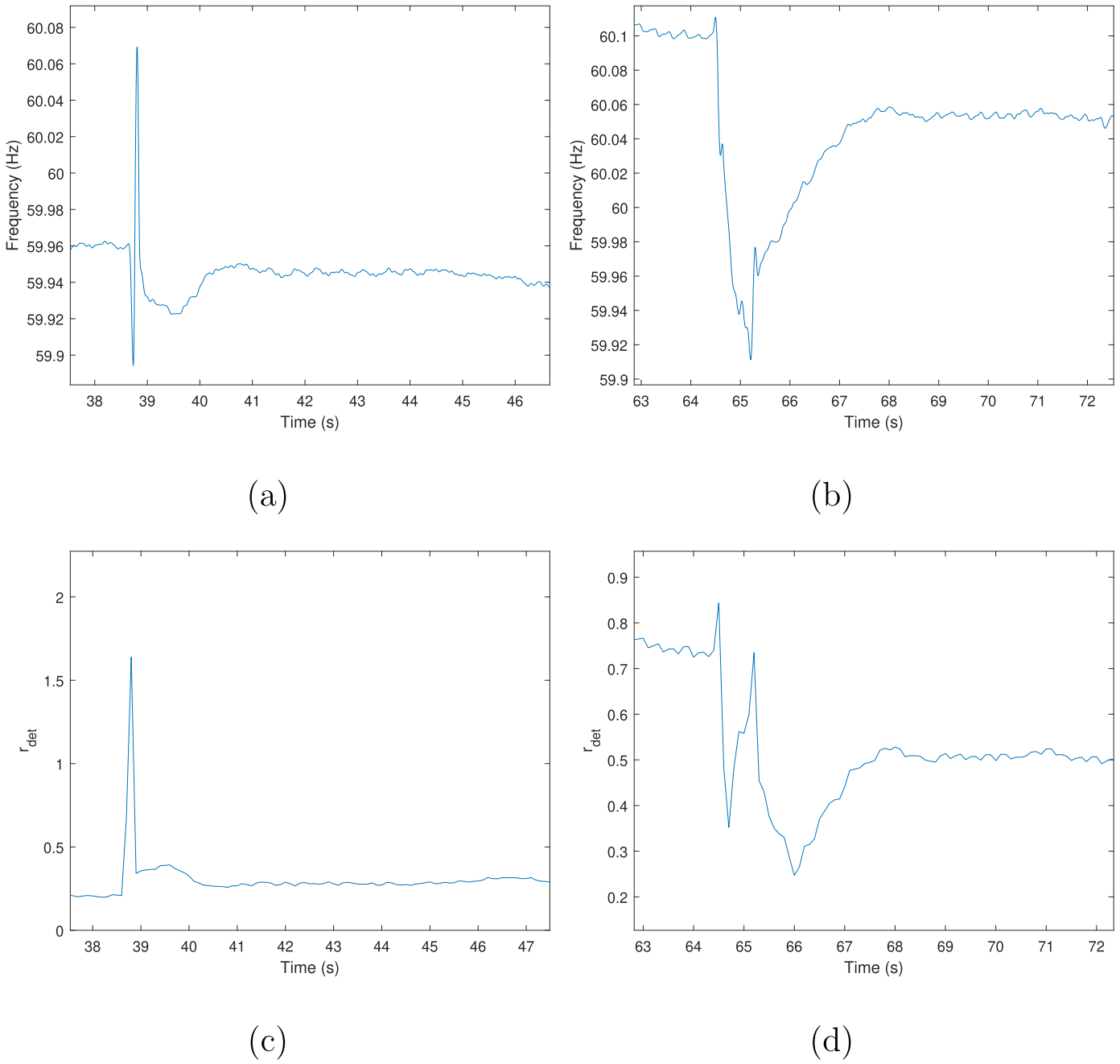


**Fig. 7.** Transient detectors and frequency test profiles: (a) Frequency response for the example hybrid arresting period event; (b) Frequency response for the example long arresting period event; (c) Transient detector response for the example hybrid arresting period event; (d) Transient detector response for the example long arresting period event.

0.3 and 0.05 s ROCOF window sizes. The initial and finalized thresholds are given in Table 1 where the initial thresholds are user defined values and the finalized thresholds are designed by the minimum ROCOFs of the detected long arresting period events. After applying the new thresholds, the long arresting period events can be captured from the raw data while the transient events are filtered out. In addition, the frequency spikes in hybrid arresting period events are also filtered out and they are captured as long arresting period events.

### 4.2. Transient detector design

In order to further distinguish the hybrid arresting period events from the long arresting period events, a transient detector [19] is designed to identify the waveform phase and voltage magnitude step change. Note that the frequency spikes are actually caused by the phase step change. The definition of the proposed transient detector, $r_{det}$, is,

$$r_{det} = \sum_{t=t_0}^{T+t_0} |U(t+T) - U(t)|, \tag{6}$$

where $t$ is the time stamp, $T$ is the transient detector window size which is defined as 1 cycle here, $t_0$ is the starting time, and $U(t)$ is the waveform voltage raw data. If distortion happens in the waveform, this detector can quickly identify the distortion and report to the proposed algorithm.

In order to verify the effectiveness of the proposed algorithm, a simulated hybrid arresting period event and a long arresting period event are deployed in an ideal power source. The events are rebuilt through both the frequency, voltage magnitude, and phase jump. The

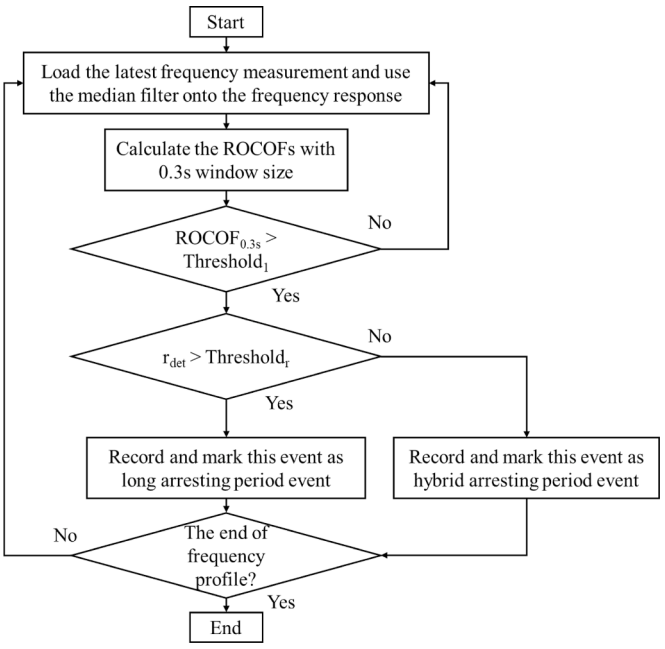


**Fig. 8.** Flowchart for event detection algorithm improved by the transient detector.

transient detectors and event frequency responses are given in Fig. 7. It can be observed that the transient detector, $r_{det}$, gives a high value feedback during the frequency spike in the example hybrid arresting event. On the other hand, this transient detector keeps in a low value during long arresting event.

As shown in Fig. 8, the event detection algorithm can be improved by using the transient detector. In this case, the hybrid arresting period events can be distinguished from the long arresting period events. When utilizing the median filter, the transient events can no longer be distinguished. Note that the transient detector is optional. The hybrid arresting period events can also be distinguished through ROCOF with 0.05 s window size before applying median filter.

## 5. Experiment results

In order to verify the effectiveness of the proposed event detection based ROCOF estimation algorithm, verifications including frequency measurement accuracy, ROCOF estimation accuracy, algorithm performance in hardware, communication protocol selection, real-world ROCOF data streaming, and field deployments in both the laboratory and the field tests are given here.

### 5.1. Algorithm deployment

UGAs are one kind of low cost, flexible, and distribution level PMU platforms [24]. With its flexibility, different kinds of synchrophasor estimation algorithms can be deployed and tested on UGAs. In this experiment, the ROCOF estimation algorithm, transient detector, and frequency estimation algorithms are deployed in the UGAs. On the other hand, the real-time ROCOFs, transient detectors, and frequency measurements can be received from the server side. For laboratory test purposes, the event detection algorithm is deployed offline in laboratory tests and deployed in the server in the field test

### 5.2. Verification in the laboratory

In the laboratory verification, the accuracy of the frequency estimation is first verified under both nominal and off-nominal frequency steady states. The results are given in Table 3. It can be observed that

**Table 3**
Frequency error under different steady state frequency level.

| Steady state frequency level | FE of UGA with 120 Hz reporting rate | FE of UGA with 10 Hz reporting rate | FE in IEEE C37.118.1 |
|---|---|---|---|
| 60 Hz | 3.8372e-05 Hz | 1.6935e-05 Hz | 0.005 Hz |
| 59.8 Hz | 3.6050e-05 Hz | 1.6648e-05 Hz | 0.005 Hz |
| 60.2 Hz | 3.8543e-05 Hz | 1.7325e-05 Hz | 0.005 Hz |

frequency error for both the nominal and off-nominal cases are much lower than the IEEE requirements (maximum frequency error is 0.005 Hz [7]) which verify the estimation accuracy of the frequency estimation. Note that the FE of UGA with a 120 Hz reporting rate is relatively lower than UGA with a 10 Hz reporting rate. This is because the accuracy of the frequency estimation is sacrificed for the higher reporting rate.

In addition, the ROCOF estimation accuracy is also verified in a laboratory. Since the estimation accuracy of the ROCOF highly depends on the ROCOF window size and the frequency noise, comparing the ROCOF estimation results under steady states would be unfair. In this case, a comparison between online ROCOF estimation and offline ROCOF calculation is given in Fig. 9. The online ROCOF estimation is using 0.3 s window size and deployed in UGA. The ROCOF estimation will be sent to the server in real-time. On the other hand, the offline ROCOF calculation is using the measured frequency to calculate the ROCOF through MATLAB curve fitting function block which can be treated as ground truth values. Experiment results shown in Fig. 9 have verified that the online ROCOF estimation can follow the offline ROCOF calculation which verifies the accuracy of the online ROCOF estimation.

### 5.3. Verification in the field test

In the field test experiment, two UGAs have been deployed in the Hawaiian Islands, i.e., the Maui and Kauai islands. The overall architecture for UGAs and servers is illustrated in Fig. 10.

In Section 4.1, the event detection and analysis for these two units have been discussed in detail. To avoid redundancy, the real-time ROCOF estimation results for the three example events (the frequency responses are shown in Fig. 6(a), (b), and (c)) which are calculated in the UGA side are given in Fig. 11. It can be observed that the ROCOFs with 0.3 and 0.05 s window sizes can be successfully calculated in the servers in real-time. Furthermore, ROCOFs with both 0.3 and 0.05 s window sizes cannot detect transient events, which verify the effectiveness of the median filter. For long and hybrid arresting period events, ROCOFs with 0.3 s window size could easily capture these two kinds of events. If a short response time is required, ROCOFs with 0.05 s window size can also be utilized to capture these two kinds of events.

TCP/IP protocol is utilized between UGAs and servers for data streaming. Since there are Coordinated Universal Time (UTC) time stamps for each frequency and ROCOF estimation, the communication delay caused by the TCP/IP protocol has no influence on the accuracy of the ROCOF estimation. However, the delay caused by the TCP/IP protocol can be a concern for real-time applications using ROCOF estimations. A comparison between IEEE C37.118.2 and IEC 61850-90-5 is discussed in [25]. The time delay of IEEE C37.118.2 with ATM OCI can reach 13.0ms from PMUs to the regional server. In this case, a local server should be deployed in Hawaii islands to apply real-time ROCOF based applications.

As a conclusion, the proposed precise ROCOF estimation algorithm is compared with the IEEE standard in [23] is illustrated in Table 4. The performance of the proposed algorithm can be evaluated through the five aspects in the table. The FE represents the frequency measurement accuracy under 120 Hz reporting rate which is much better than the requirements in the IEEE standard. The rate of frequency error (RFE) represents the accuracy of the ROCOF estimation which is also much better than the IEEE standard requirement. Since the ROCOF in this paper is targeting on the initial ROCOF estimation, the window size is

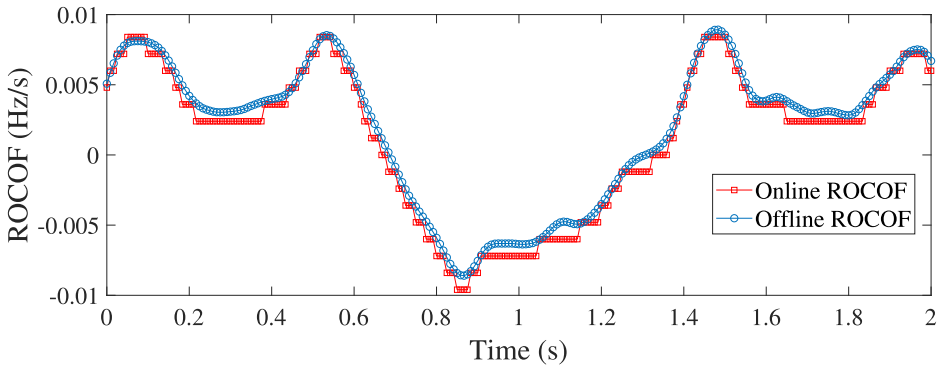


**Fig. 9.** ROCOF estimation comparison between online and offline calculation.

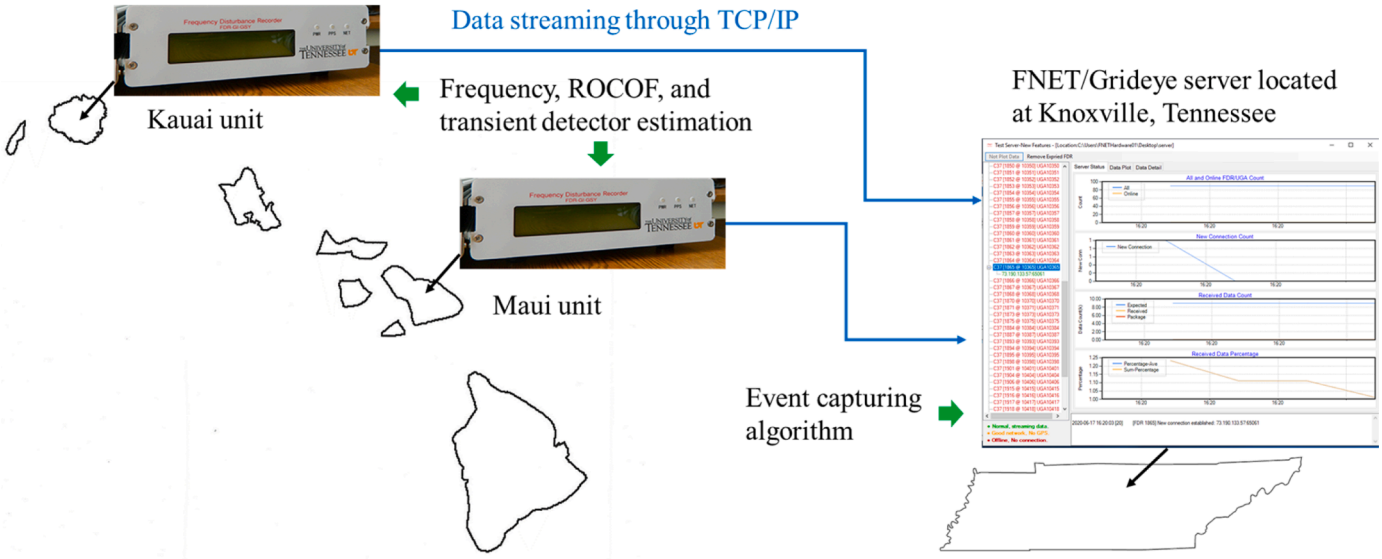


**Fig. 10.** The experiment setup in the field test.

flexible based on the Hawaii island power grid while this is not required in IEEE standard so that it is uniquely designed in this paper. The algorithm is deployed in UGAs which utilize TCP-IP protocols to communicate and it is one of the available communication protocols in the IEEE standard. Finally, in the field deployment, the data missing rate is lower than 3% which is very good in real-world applications and there is no requirement in IEEE standard. To summarize, the proposed algorithm and the deployment in UGAs can fully fulfill the requirements in IEEE standard. In addition, it has a uniquely designed ROCOF window and a very good data missing rate in the field deployment.

## 6. Conclusions

ROCOF measurement is critical for high-renewable low-inertia power grid as it is an important indicator of frequency stability and can help predict the magnitude of disturbances. This paper introduces a precise ROCOF estimation algorithm for low inertia power grids. The ROCOF estimation algorithm is calculated by a LSM based curve fitting method on the frequency response during a given window size. By utilizing the real-world historical data, the ROCOF thresholds and window sizes are optimized. The proposed ROCOF estimation algorithm can precisely estimate the initial ROCOF for a generation trip event. Furthermore, a transient detector is also designed to distinguish the hybrid arresting period events. Laboratory and field tests with onsite SMDs demonstrate the effectiveness of the proposed algorithm and frequency estimation.

## Acknowledgment

This work was authored in part by the National Renewable Energy Laboratory, operated by Alliance for Sustainable Energy, LLC, for the U. S. Department of Energy (DOE) under Contract No. DE-AC36-08GO28308. Funding provided by U.S. Department of Energy Office of Energy Efficiency and Renewable Energy Solar Energy Technologies Office Award Number 37772. The views expressed in the article do not necessarily represent the views of the DOE or the U.S. Government. The U.S. Government retains and the publisher, by accepting the article for publication, acknowledges that the U.S. Government retains a nonexclusive, paid-up, irrevocable, worldwide license to publish or reproduce the published form of this work or allow others to do so, for U.S. Government purposes.

## CRediT authorship contribution statement

**He Yin:** Writing – review & editing. **Yuru Wu:** Validation. **Wei Qiu:** Writing – review & editing. **Chujie Zeng:** Validation. **Shutang You:** Methodology. **Jin Tan:** Funding acquisition. **Andy Hoke:** Funding acquisition. **Cameron J. Kruse:** Data curation. **Brad W. Rockwell:** Data curation. **Kelcie Ann Kawamura:** Data curation. **Yilu Liu:** Project administration.

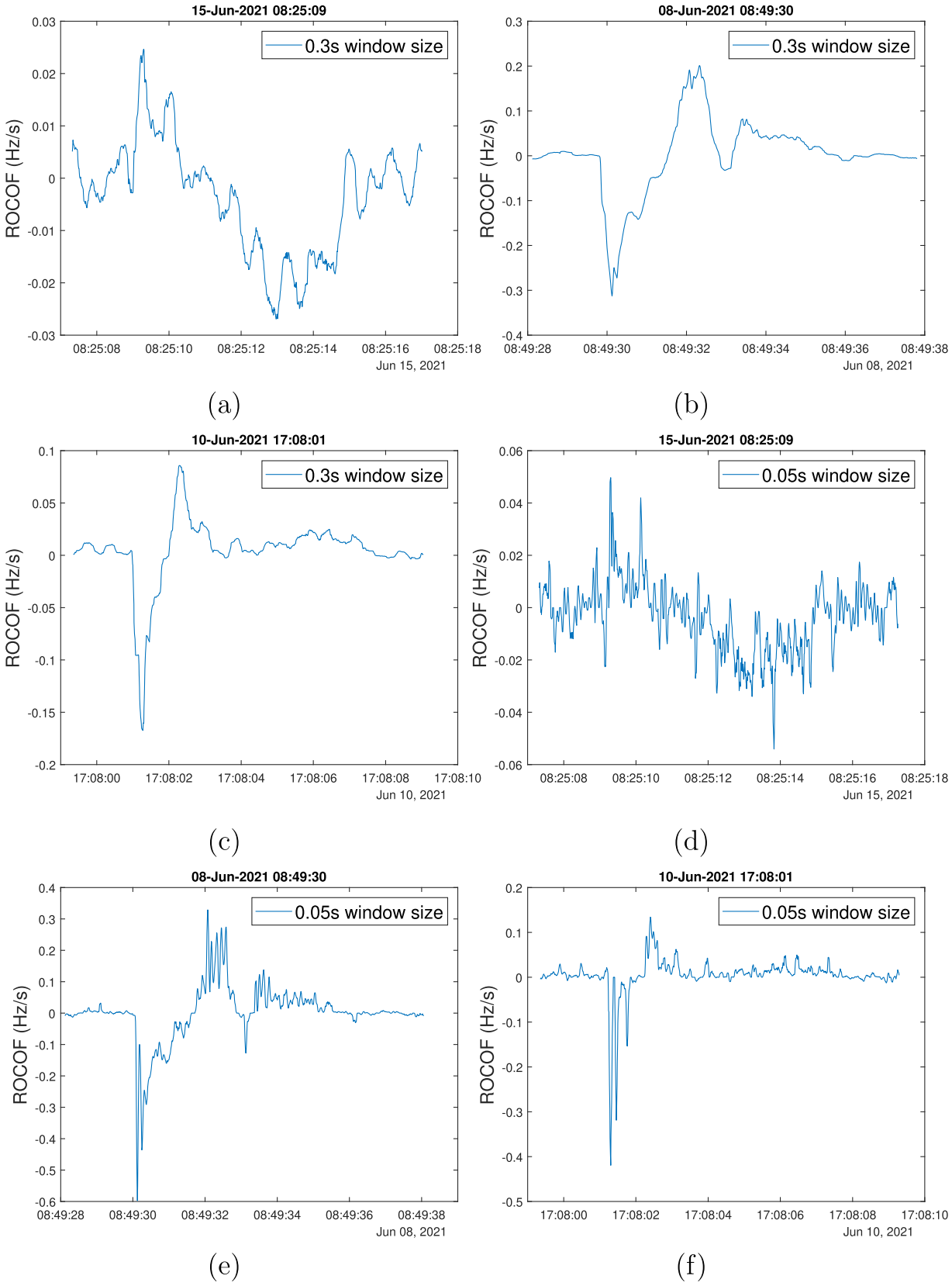


**Fig. 11.** Example ROCOF estimated during events in the Hawaiian Islands: (a) ROCOF with 0.3 s window size during a transient event; (b) ROCOF with 0.3 s window size during a long arresting period event; (c) ROCOF with 0.3 s window size during a hybrid arresting period event; (d) ROCOF with 0.05 s window size during a transient event; (e) ROCOF with 0.05 s window size during a long arresting period event; (f) ROCOF with 0.05 s window size during a hybrid arresting period event;

**Table 4**
Performance Comparison between proposed algorithm and IEEE Standard.

| Algorithms | FE under 120 Hz Report. Rate | RFE under 1 $Hz/s$ ramp test | ROCOF window | Communication protocol | Data missing rate |
|---|---|---|---|---|---|
| Proposed algorithm | 3.8372e-05 Hz | 3e-2 $Hz/s$ | Flexible | TCP-IP | $< 3\%$ |
| IEEE Standard | 5e-03 Hz | 0.1 $Hz/s$ | No req. | TCP-IP or UDP or series port | No req. |

## Declaration of Competing Interest

The authors declare that they have no known competing financial interests or personal relationships that could have appeared to influence the work reported in this paper.

## References


[1] D.P. Chassin, Z. Huang, M.K. Donnelly, C. Hassler, E. Ramirez, C. Ray, Estimation of WECC system inertia using observed frequency transients, IEEE Trans. Power Syst. 20 (2) (2005) 1190–1192.

[2] M. Sun, G. Liu, M. Popov, V. Terzija, S. Azizi, Underfrequency load shedding using locally estimated ROCOF of the center of inertia, IEEE Trans. Power Syst. (2021).

[3] H.R. Chamorro, F.R.S. Sevilla, F. Gonzalez-Longatt, K. Rouzbehi, H. Chavez, V. K. Sood, Innovative primary frequency control in low-inertia power systems based on wide-area ROCOF sharing, IET Energy Syst. Integr. 2 (2) (2020) 151–160.

[4] R. Ilievska, R. Mihalic, E. Kushnikov, J. Zakonjsek, U. Rudez, Hardware-in-the-loop testing of an intelligent electronic device for innovative UFLS protection. 2021 IEEE Madrid PowerTech, IEEE, 2021, pp. 1–5.

[5] W. Wang, H. Yin, C. Chen, A. Till, W. Yao, X. Deng, Y. Liu, Frequency disturbance event detection based on synchrophasors and deep learning, IEEE Trans. Smart Grid 11 (4) (2020) 3593–3605.

[6] Y. Zhang, P. Markham, T. Xia, L. Chen, Y. Ye, Z. Wu, Z. Yuan, L. Wang, J. Bank, J. Burgett, R.W. Conners, Y. Liu, Wide-area frequency monitoring network (FNET) architecture and applications, IEEE Trans. Smart Grid 1 (2) (2010) 159–167, https://doi.org/10.1109/TSG.2010.2050345.

[7] IEEE, IEEE standard for synchrophasor measurements for power systems. IEEE Std C37.118.1-2011 (Revision of IEEE Std C37.118-2005), 2011, pp. 1–61, https://doi.org/10.1109/IEEESTD.2011.6111219.

[8] F. Wilches-Bernal, J. Wold, R. Concepcion, J. Budai, A method for correcting frequency and ROCOF estimates of power system signals with phase steps. 2019 North American Power Symposium (NAPS), 2019, pp. 1–6, https://doi.org/10.1109/NAPS46351.2019.9000204.

[9] P.S. Wright, P.N. Davis, K. Johnstone, G. Rietveld, A.J. Roscoe, Field measurement of frequency and ROCOF in the presence of phase steps, IEEE Trans. Instrum. Meas. 68 (6) (2018) 1688–1695.

[10] A.K. Singh, B.C. Pal, Rate of change of frequency estimation for power systems using interpolated DFT and Kalman filter, IEEE Trans. Power Syst. 34 (4) (2019) 2509–2517.

[11] G. Frigo, A. Derviškadić, Y. Zuo, M. Paolone, PMU-based ROCOF measurements: Uncertainty limits and metrological significance in power system applications, IEEE Trans. Instrum.Meas. 68 (10) (2019) 3810–3822.

[12] P. Romano, M. Paolone, Enhanced interpolated-DFT for synchrophasor estimation in FPGAs: theory, implementation, and validation of a PMU prototype, IEEE Trans. Instrum.Meas. 63 (12) (2014) 2824–2836.

[13] A. Derviškadić, P. Romano, M. Paolone, Iterative-interpolated DFT for synchrophasor estimation: a single algorithm for p-and m-class compliant PMUs, IEEE Trans. Instrum.Meas. 67 (3) (2017) 547–558.

[14] M. Bertocco, G. Frigo, C. Narduzzi, C. Muscas, P.A. Pegoraro, Compressive sensing of a Taylor-Fourier multifrequency model for synchrophasor estimation, IEEE Trans. Instrum.Meas. 64 (12) (2015) 3274–3283.

[15] A. Arana, et al., Fast frequency response concepts and bulk power system reliability needs. NERC Inverter-Based Resource Performance Task Force (IRPTF), 2020.

[16] P.V. Brogan, R.J. Best, D.J. Morrow, K. McKinley, M.L. Kubik, Effect of bess response on frequency and ROCOF during underfrequency transients, IEEE Trans. Power Syst. 34 (1) (2019) 575–583, https://doi.org/10.1109/TPWRS.2018.2862147.

[17] C. Zhang, X. Dou, Z. Zhang, G. Lou, F. Yang, G. Li, Inertia-enhanced distributed voltage and frequency control of low-inertia microgrids, IEEE Trans. Power Syst. (2021), https://doi.org/10.1109/TPWRS.2021.3057078.1–1

[18] L. Zhan, Y. Liu, J. Culliss, J. Zhao, Y. Liu, Dynamic single-phase synchronized phase and frequency estimation at the distribution level, IEEE Trans. Smart Grid 6 (4) (2015) 2013–2022, https://doi.org/10.1109/TSG.2015.2400973.

[19] L. Zhan, B. Xiao, F. Li, H. Yin, W. Yao, Z. Li, Y. Liu, Fault-tolerant grid frequency measurement algorithm during transients, IET Energy Syst. Integr. 2 (3) (2020) 173–178.

[20] FNET, http://fnetpublic.utk.edu/tabledisplay.html(2021).

[21] M. Grebla, J.R. Yellajosula, H.K. Høidalen, Adaptive frequency estimation method for ROCOF islanding detection relay, IEEE Trans. Power Deliv. 35 (4) (2019) 1867–1875.

[22] Y. Liu, Y. Cui, W. Yu, Y. Zhang, L. Wu, S. You, Y. Liu, Recent application examples of FNET/GridEye. 2018 IEEE 12th International Conference on Compatibility, Power Electronics and Power Engineering (CPE-POWERENG 2018), 2018, pp. 1–6, https://doi.org/10.1109/CPE.2018.8372494.

[23] IEEE/IEC international standard - measuring relays and protection equipment - Part 118-1: synchrophasor for power systems - measurements, IEC/IEEE 60255-118-1:2018, 2018, pp. 1–78, https://doi.org/10.1109/IEEESTD.2018.8577045.

[24] H. Yin, W. Yao, L. Zhan, W. Yu, J. Zhao, Y. Liu, Low cost, flexible, and distribution level universal grid analyser platform: designs and implementations, IET Gener. Transm. Distrib. 14 (19) (2020) 3945–3952.

[25] I. Ali, M.A. Aftab, S.M.S. Hussain, Performance comparison of IEC 61850-90-5 and IEEE c37.118.2 based wide area PMU communication networks, J. Mod. Power Syst. Clean Energy 4 (3) (2016) 487–495, https://doi.org/10.1007/s40565-016-0210-y.